Applied Catalysis B: Environmental 224 (2018) 579–585

Contents lists available at ScienceDirect

Applied Catalysis B: Environmental

journal homepage: www.elsevier.com/locate/apcatb

Inhibiting competing reactions of iodate/iodide redox mediators by surface modification of photocatalysts to enable Z-scheme overall water splitting

Yu Qi[a,b], Shanshan Chen[a], Junyan Cui[a,c], Zhiliang Wang[a], Fuxiang Zhang[a,*], Can Li[a,*]

[a] State Key Laboratory of Catalysis, iChEM, Dalian Institute of Chemical Physics, Chinese Academy of Sciences, Dalian National Laboratory for Clean Energy, Dalian, 116023, China

[b] University of Chinese Academy of Sciences, Beijing 100049, China

[c] Key Laboratory of Surface and Interface Chemistry of Jilin Province, College of Chemistry, Jilin University, Changchun 130021, China

ARTICLE INFO

Keywords:
Overall water splitting
Photocatalysis
Z-scheme
Surface modification
(Oxy)Nitride

ABSTRACT

Construction of photocatalytic Z-scheme overall water splitting (OWS) using iodate/iodide (IO_3^-/I^-) redox mediator commonly confronts challenges of competing reactions and slow reaction kinetics. Here we address the aforementioned key issues using surface modification strategy. Visible-light-responsive tantalum nitride (Ta_3N_5) and tantalum oxynitride (TaON) are employed as the O_2- and H_2-evolving photocatalysts, respectively. It is found that the inhibition of competing reactions and promotion of half reactions are indispensable for the successful construction of Z-scheme OWS system, both of which are directly related to the surface property of the photocatalysts. Specifically, the magnesia modification on the surface of Ta_3N_5 is demonstrated to be effective not only in suppressing the adsorption and oxidation of I^- ions (a competing reaction of water oxidation), but also in promoting the charge separation and O_2-evolving rate via meliorative dispersion of loaded iridium cocatalyst. And surface coating of Cr_2O_3 nanolayer on the platinum cocatalyst loaded on the TaON-based photocatalyst is available to inhibit the reduction of IO_3^- ions (a competing reaction of proton reduction) and improve the H_2-evolving rate. Only after both inhibition of competing reactions and promotion of H_2- and O_2-evolving reactions under the assistance of surface modification, the visible-light-driven Z-scheme OWS system can be achieved successfully with the mixture of IO_3^- and I^- ions as a redox mediator. This work sheds light on the availability and importance of surface modification strategy in fabricating Z-scheme OWS system.

1. Introduction

Photocatalytic overall water splitting (OWS) into H_2 and O_2 using particulate photocatalyst is one of the promising ways of converting solar energy into chemical energy [1–7]. Based on the photoexcitation number, the particulate photocatalytic OWS systems can be generally divided into one-step and two-step (also called as Z-scheme) types [8]. As for the one-step approach, conduction band minimum and valence band maximum of the semiconductor are strictly required to straddle the potentials of proton reduction and water oxidation reactions, so only limited semiconductors have been reported to drive the one-step OWS system under visible light irradiation [8–10]. Comparatively, for the construction of Z-scheme system, the energy bands of the semiconductors are only required to drive the proton reduction or water oxidation reaction, so the candidate materials can be broadened.

A typical Z-scheme OWS system, except for some Z-scheme systems with solid state electron mediators, is commonly composed of H_2-evolving photocatalyst (HEP), O_2-evolving photocatalyst (OEP) and an aqueous redox mediator [11–13]. Abe et al. reported the first example of photocatalytic Z-scheme OWS system in 2001 [14]. Afterwards, continuous efforts have been made to construct new systems by developing effective redox mediators and/or new photocatalysts with an additional effort to use the wide wavelength range of visible light absorption [15–29]. Meanwhile, the IO_3^-/I^- redox shuttle has been given to be one of the most extensive attention due to its suitable redox potential and no absorption competition of visible light [15–20,23,24,26]. Scheme 1 shows the schematic diagram of typical IO_3^-/I^- mediator-based Z-scheme OWS system. In the O_2-evolving side, the desirable reactions occur as follows:

$$2H_2O + 4\,h^+ \rightarrow O_2 + 4H^+ \quad (1)$$

$$IO_3^- + 6e^- + 3H_2O \rightarrow I^- + 6OH^- \quad (2)$$

On the other hand, the desirable reactions occur in the H_2-evolving side as follows,

$$2H^+ + 2e^- \rightarrow H_2 \quad (3)$$

* Corresponding authors.
E-mail addresses: fxzhang@dicp.ac.cn (F. Zhang), canli@dicp.ac.cn (C. Li).

http://dx.doi.org/10.1016/j.apcatb.2017.10.041
Received 30 August 2017; Received in revised form 12 October 2017; Accepted 14 October 2017
Available online 16 October 2017
0926-3373/

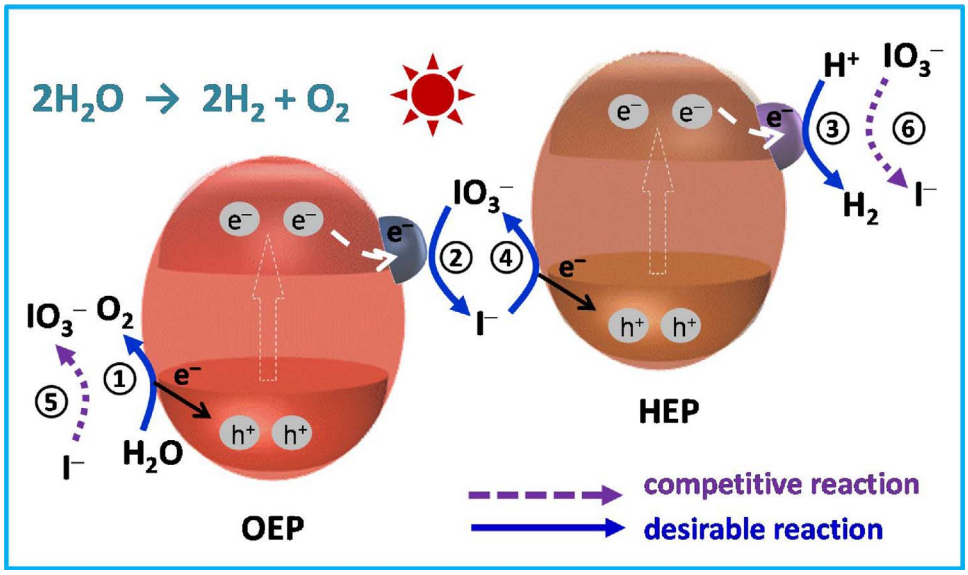

Scheme 1. Schematic diagram of typical Z-scheme OWS system.

$$I^- + 6\,h^+ + 3H_2O \rightarrow IO_3^- + 6H^+ \quad (4)$$

However, the thermodynamically advantageous competing reactions will proceed preferentially over the photocatalysts (reaction 5 and 6 in Scheme 1). As described in Scheme 1, the overall water splitting can be driven only when the following parameters are simultaneously satisfied: i) the excited electrons on the surface of OEP can be used for reduction of IO_3^-, ii) the electrons of I^- ions can be effectively transferred to the HEP; iii) both HEP and OEP are active for H_2 and O_2 evolution, respectively. If anyone of them does not work well, the overall water splitting will not happen. Based on the above analysis, it is easy to understand that if just employing I^- ions to drive the overall water splitting, it requires that the OEP is highly active to transfer excited electrons to the IO_3^- ions with extremely low concentration which are *in situ* formed by the photo-oxidation of I^- ions on the surface of HEP. As a matter of fact, only few photocatalysts like WO_3 or rutile TiO_2 have been reported to be active in the extremely low concentration of IO_3^- ions *in situ* formed [15,16,23,30–32]. However, the absorption edge of rutile TiO_2 or WO_3 material is short, restricting the theoretical solar energy conversion efficiency of two-step OWS system. Accordingly, it is highly desirable to develop novel OEPs with wider visible light wavelength response, especially reaching 600 nm, to replace the conventional WO_3 or TiO_2 [33]. To reach this goal, one possible strategy is to employ the mixture of IO_3^- and I^- ions instead of single I^- ions as the shuttle ions. In this case, it may well overcome the infeasible reduction of IO_3^- ions with extremely low concentration on the OEP. However, it confronts new challenge that the reduction of IO_3^- ions and oxidation of I^- ions with enhanced concentration will compete with the proton reduction and water oxidation reaction, respectively. In the O_2-evolving side, the OEP will prefer to oxidizing I^- ions (the reaction 5 in Scheme 1) rather than oxidizing water molecules (the reaction 1 in Scheme 1) due to thermodynamics disadvantage of water oxidation with respect to the oxidation of I^- ions [13].

Similarly, the competing reaction will also happen in the H_2-evolving side. If the IO_3^- ions *in situ* formed by the HEP is not reduced by the OEP rapidly, the reduction of residual IO_3^- ions (the reaction 6 in Scheme 1) will compete with the proton reduction (the reaction 3 in Scheme 1) on the surface of HEP because the reduction of IO_3^- ions is more favorable to happen compared to the reduction of proton from the view point of thermodynamics. Accordingly, inhibition of the competing reactions caused by the shuttle ions is crucial for the fabrication of Z-scheme OWS system as well as its reaction kinetics. Thus, suitable strategies should be developed to solve the undesirable competing reactions. However, to date, the specific discussion on the inhibition of competing reactions is still shortage.

In this work, we will give a discussion on how to construct an effective Z-scheme OWS system by suppressing the competing reactions caused by IO_3^-/I^- shuttle ions. As a model illustration, Ta_3N_5 (E_g: 2.1 eV) and TaON (E_g: 2.4 eV), both of which own absorption edges of over 500 nm, are employed as an OEP and a HEP, respectively. Here the especial emphasis is paid on the influence of surface modification on the inhibition of competing reactions as well as reaction kinetics of both half reactions.

2. Experimental

2.1. Synthesis of the OEP and HEP

Pristine Ta_3N_5 and MgO modified Ta_3N_5 (denoted as MgO/Ta_3N_5) samples were employed to prepare the OEPs. The pristine Ta_3N_5 was synthesized through heating Ta_2O_5 powder under an NH_3 flow (250 mL/min) at 1223 K for 15 h. MgO/Ta_3N_5 was synthesized according to our previous work [34]. Typically, 0.2 g Ta_3N_5 powder was dispersed in a calculated amount of $MgSO_4$ aqueous solution with ultrasonic agitation for *ca.* 5 min and then dried in a water bath at 353 K, and subsequently the dried mixture was treated at 973 K for 0.5 h under an NH_3 flow (250 mL/min). The mass ratio of MgO:Ta_3N_5 was adjusted for the performance optimization by changing the content of $MgSO_4$ precursor. The ZrO_2 modified TaON (denoted as ZrO_2/TaON) was synthesized by nitriding the ZrO_2/Ta_2O_5 under an NH_3 flow (20 mL/min) at 1123 K for 15 h [16].

2.2. Deposition of cocatalysts

As for the iridium deposition, the conventional impregnation and subsequent H_2 reduction treatment was adopted [35]. Typically, 0.2 g Ta_3N_5 or MgO/Ta_3N_5 sample was immersed in a calculated amount of K_2IrCl_6 aqueous solution with ultrasonic agitation for *ca.* 5 min. After the solution was completely evaporated in a water bath at 353 K, the impregnated powder was collected and reduced at 473 K for 1 h under a flow of 5% H_2/Ar (200 mL/min).

Similarly, the deposition of platinum cocatalyst on the surface of the HEP was also carried out by impregnation and subsequent H_2 reduction treatment. If needed, Cr_2O_3 was then photodeposited on the surface of platinum to form core/shell (Pt/Cr_2O_3) structure [36]. H_2PtCl_6 and K_2CrO_4 were employed as the precursors for the deposition of platinum

and Cr_2O_3, respectively. The photodeposition of Cr_2O_3 was carried out using methanol as a hole scavenger under the full-spectral irradiation of 300 W Xe lamp for 6 h. After the photodeposition, the final product was centrifuged and washed with distilled water, then dried overnight at 353 K.

2.3. Preparation of electrodes

As for the measurement of contact angle (CA), Ta_3N_5-based films ($2 \times 3\ cm^2$) were prepared on FTO substrate by electrophoretic deposition (EPD). Typically, the EPD was carried out in an acetone solution (50 mL) containing powder sample (50 mg) and iodine (20 mg), which was dispersed by sonication for 20 min. The FTO electrode was immersed, paralleling with another FTO electrode, and the distance between these two electrodes was 1 cm 20 V and 1 A were applied for 3 min (10 s at one time) using a potentiostat (ITECH IT6834), then the prepared films were dried at 333 K for 12 h before the CA measurement.

As for the *I–V* measurement, ZrO_2/TaON films ($1 \times 2\ cm^2$) were also prepared by the EPD method [37]. The substrate changes to the Ti foil, and the procedure is the same except that the powder weight increases to 75 mg and the deposition time is reduced to 2 min. Then the films were dried at 353 K overnight. 20 mM $TaCl_5$ solution dissolved into anhydrous methanol was dropped onto the film with 10 μL/cm^2 for five times. The dried electrode was then calcinated at 873 K (5 K/min) for 1 h under an NH_3 flow (100 mL/min). Afterwards, the platinum was deposited on the as-obtained films by dropping a calculated amount of H_2PtCl_6 aqueous solution, and treated at 473 K for 15 min under a flow of 5% H_2/Ar (200 mL/min) for the reduction of platinum. If needed, the Cr_2O_3 was further photodeposited to produce core/shell structure (Pt/Cr_2O_3) via full-spectral irradiation in the K_2CrO_4-containing aqueous solution.

For the electrochemical measurement, a platinum plate was used as a counter electrode and the Ag/AgCl electrode was used as a reference electrode. The as-prepared electrode was separated from the Pt electrode through an ion-exchange membrane (Nafion). The Na_2SO_4 (0.1 M) with or without 5 mM $NaIO_3$ aqueous solution were used as an electrolyte. The potential of the working electrode was controlled by a potentiostat. Before the measurement, the solution was purged with argon gas [18].

3. Results and discussion

3.1. O_2-evolving reaction and inbibition of I^- ions oxidation

The photocatalytic water oxidation reaction on the pristine Ta_3N_5 or MgO/Ta_3N_5 with iridium loaded as cocatalyst was carried out using $NaIO_3$ as an electron acceptor under visible light irradiation ($\lambda \geq 420$ nm). Meanwhile, the function of the cocatalyst iridium was to accumulate the photogenerated electrons and accelerate the reduction of IO_3^- ions. The basic processes for O_2 evolution can be described as following equations of 1 and 2 as Scheme 1 shows.

$$\text{Photocatalyst} + h\nu\ (> \text{band gap energy}) \rightarrow e^- + h^+$$

$$2H_2O + 4h^+ \rightarrow O_2 + 4H^+ \quad (1)$$

$$IO_3^- + 6e^- + 3H_2O \rightarrow I^- + 6OH^- \quad (2)$$

As expected, no reaction occurs in the dark, and the water oxidation for O_2 evolution just happens under the illumination of visible light. The influence of magnesia content on the O_2 evolution rate was first examined. As shown in Fig. 1a, a volcano-type dependence curve of initial O_2 evolution rates as a function of magnesia content is observed, among which the maximum rate of 164 μmol/h can be obtained on the Ir–5 *wt*% MgO/Ta_3N_5 sample. The activity on the optimized MgO-modified sample (if it is not specially stated, the MgO/Ta_3N_5 appearing hereafter refers to 5 *wt*% MgO/Ta_3N_5) is over six times higher than that of pristine Ir-Ta_3N_5, demonstrating the availability of magnesia modification in promoting the O_2 evolution rate. Fig. S1 gives its time course of water oxidation, in which the decrease of O_2 evolution rate might be ascribed to the decrease of IO_3^- ions concentration during reaction [13]. Fig. S2 shows the activity results of cut-off wavelength, from which not only the water oxidation activity can be confirmed to be driven by visible light according to their similar trend between activity and wavelength absorption, but also the visible light utilization of Ta_3N_5 photocatalyst in the iodate system is found to be beyond 550 nm, much longer than the widely reported WO_3 (below 450 nm) [38].

Basically, oxidation of I^- ions (E^o = 1.08–0.059 pH, V versus NHE) is easier than the water oxidation (E^o = 1.23–0.059 pH, V versus NHE), so the oxidation of I^- ions (the reaction 5 in Scheme 1) will compete with the water oxidation (the reaction 1 in Scheme 1) to consume photogenerated holes [11]. As shown in Fig. 1b, the existence of I^- ions in the reaction solution does really cause a general decrease of O_2 evolution rate on both pristine Ir-Ta_3N_5 and Ir-MgO/Ta_3N_5 samples and the decline will increase with increasing the concentration of I^- ions, indicating the existence of competing reaction. Comparatively, the Ir-MgO/Ta_3N_5 sample shows an effective inhibition effect on the competing reaction compared to the pristine sample. When the decline comes to the steady state (adding 1 mM NaI), 5% of the O_2 evolution rate on the pristine Ir-Ta_3N_5 sample will be kept, while more than 40% of the O_2 evolution rate will be maintained for the Ir-MgO/Ta_3N_5 sample. That is to say, the percentages of the photogenerated holes used for the I^- ions oxidation rather than water oxidation on the Ir-Ta_3N_5 and Ir-MgO/Ta_3N_5 photocatalysts are 95% and 60%, respectively. It demonstrates that the magnesia modification can suppress the competing reaction to a certain degree.

The reaction kinetics of water oxidation was analyzed on the optimized sample by changing the concentration of the electron acceptor of $NaIO_3$. As shown in Fig. 1c, the O_2 evolution rate is strongly dependent on the concentration of $NaIO_3$. In the concentration range of 0–2 mM, the O_2-evloving rate almost linearly increases and the initial reaction rate of the Ir-MgO/Ta_3N_5 sample is about thirteen times of that of the pristine Ir-Ta_3N_5, further revealing the importance of magnesia modification in promoting the water oxidation. The increasing dependence curve of activity reveals that the increase of $NaIO_3$ concentration is favorable for the water oxidation kinetics.

In order to get insight into the inhibition of competing reaction and promotion of the photocatalytic performance, the pristine Ta_3N_5 and MgO/Ta_3N_5 were firstly characterized by XRD, UV–vis DRS and surface area measurement. The magnesia modification is found to make little effect on the structure of Ta_3N_5 such as crystallization (Fig. S3A) and morphology (Fig. S3 B and C). Both of the samples exhibit a visible absorption edge of *ca.* 600 nm and similar absorption backgrounds (Fig. S4) originating from the formation of reduced tantalum species (e.g., Ta^{4+} ions) [15,16]. Based on their SEM images in Fig. S3 B and C, the average sizes of Ta_3N_5-based samples are both in the region of $0.4 - 1.0\ \mu m$. As demonstrated by CA measurement (Fig. S5), the surface of Ta_3N_5 tends to be modulated from hydrophobic feature for the pristine Ta_3N_5 into hydrophilic one for the MgO/Ta_3N_5 sample, similar to our previous observation [34].

Considering that the magnesia modification has little effect on the structure and morphology of Ta_3N_5, we pay special attention to the influence of the magnesia modification on the structures of the deposited iridium cocatalyst and the adsorption of I^- ions. It is found that the magnesia mainly exists as nano-islands on the surface of Ta_3N_5 according to the TEM observation of Fig. S6. The deposited Ir nanoparticles are mainly distributed on the surface of Ta_3N_5 and MgO, respectively. The size and dispersion of deposited Ir nanoparticles on the surface of pristine Ta_3N_5 and MgO/Ta_3N_5 samples are remarkably different (Fig. 2 and S7). As seen in the FESEM images, the deposited Ir nanoparticles on the surface of Ta_3N_5 tend to be aggregated (Fig. S7a), while they are more homogeneously dispersed on the MgO/Ta_3N_5

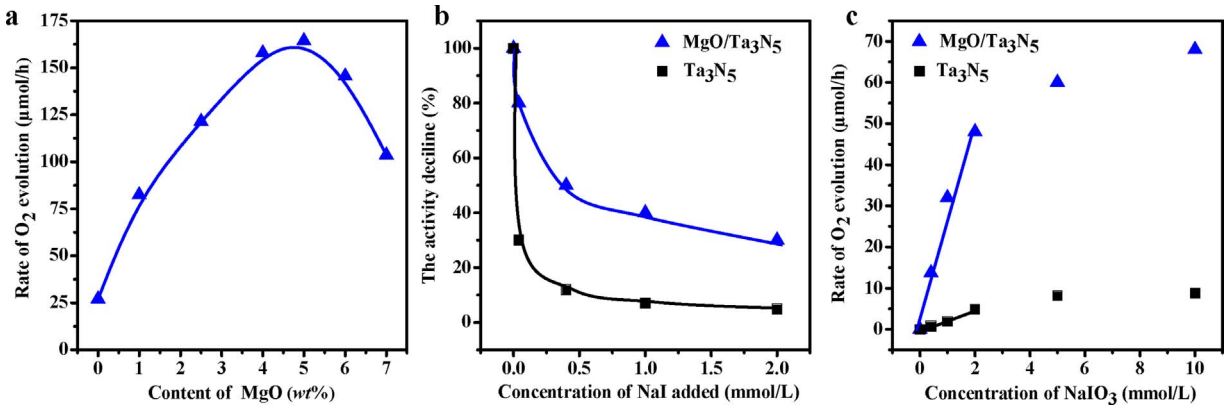

Fig. 1. (a) Rates of O_2 evolution on the Ta_3N_5-based photocatalysts as a function of magnesia content[a]. (b) Influence of NaI added on the O_2-evolving activity of Ta_3N_5-based photocatalysts with and without magnesia modification[b]. (c) O_2-evolving reaction kinetics as a function of IO_3^- concentrations on the Ta_3N_5- and MgO/Ta_3N_5-based photocatalysts[c].
[a] Reaction conditions: 0.15 g catalyst; 1 *wt*% Ir loaded; aqueous $NaIO_3$ solution (150 mL, 5 mM); 300 W xenon lamp (λ ≥ 420 nm), Pyrex top-irradiation type, 1 h reaction time.
[b] Reaction conditions: 0.15 g catalyst; 1 *wt*% Ir loaded; aqueous $NaIO_3$ solution (150 mL, 5 mM) with different concentrations of NaI; 300 W xenon lamp (λ ≥ 420 nm), Pyrex top-irradiation type, 1 h reaction time.
[c] Reaction conditions: 0.04 g catalyst; 1 *wt*% Ir loaded; aqueous $NaIO_3$ solution (100 mL); 300 W xenon lamp (λ ≥ 420 nm), Pyrex top-irradiation type, 1 h reaction time.

sample (Fig. S7b). Based on the TEM images in Fig. 2a and b, the particle size of deposited Ir on the surface of pristine Ta_3N_5 and MgO/Ta_3N_5 samples is mainly located in the range of about 5–20 nm (Fig. 2a) and 2–4 nm (Fig. 2b), respectively. The improved dispersion and decreased particle size of the deposited Ir particles on the MgO/Ta_3N_5 sample are similar to our previous reported result [35], and it has been ascribed to the wettability modulation of Ta_3N_5 surface from hydrophobicity to hydrophilicity due to the magnesia modification. As the deposited iridium is requisite for the activation and reduction of IO_3^- ions to consume the photogenerated electrons, the decrease of particle size of iridium is expected to provide more active sites for promoted reduction of IO_3^- ions. What's more, the time-resolved infrared spectrum (TRIR) also demonstrates that the Ir-MgO/Ta_3N_5 sample shows prolonged lifetime of carriers compared to the pristine Ir-Ta_3N_5 (Fig. S8). Accordingly, the promoted charge separation and increased active sites should be responsible for the promoted O_2-evolving rate (Fig. 1a).

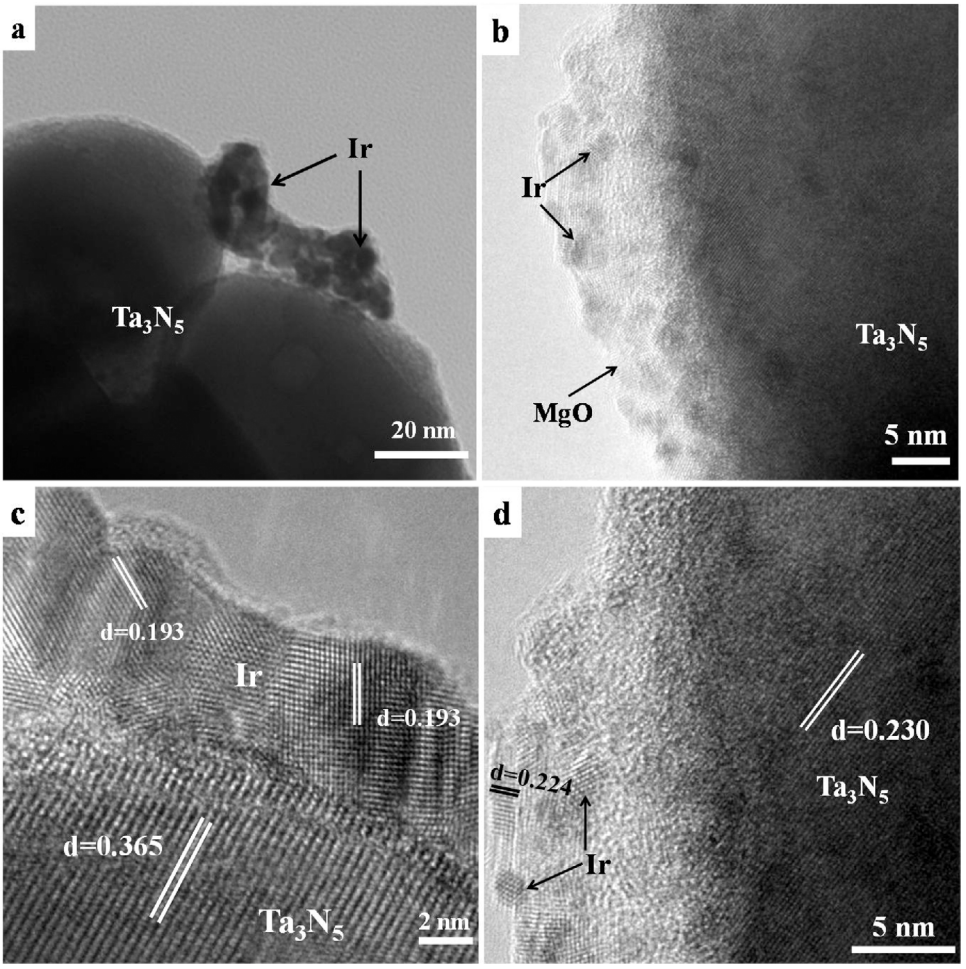

Fig. 2. TEM (a,b) and HRTEM (c,d) images of Ir-Ta_3N_5 and Ir-MgO/Ta_3N_5 samples: (a,c) 1.0 *wt*% Ir-Ta_3N_5 and (b,d) 1.0 *wt*% Ir-MgO/Ta_3N_5.

It needs to be pointed out that the magnesia itself is inert and unfavorable for direct carrier transfer, so the photogenerated electrons must tunnel the magnesia nanolayer for further reaction. Therefore, an excessive amount of deposited magnesia not only enhances its thickness leading to an inefficient electron tunnel, but also covers more surface of Ta_3N_5 causing the decreased active sites of O_2 evolution. As a result, the sample with the magnesia amount of 5 *wt*% exhibits the optimal activity (Fig. 1a). Moreover, according to the lattice spacing of loaded iridium nanoparticles given in the HRTEM images (Fig. 2c and d), the deposited iridium can be confirmed to exist as metallic nano-crystals on both samples. The metallic state of deposited iridium can be further supported by the binding energies (*ca.* 61 eV) of Ir $4f_{7/2}$ XPS spectra in Fig. S9 [39]. Additionally, the binding energies of the Ir 4*f* peaks on the Ir-MgO/Ta_3N_5 sample are a little higher than those on the Ir-Ta_3N_5. The shift of binding energy may originate from the formation of possible Ir-O bonds at the MgO-Ir interface and/or the smaller particle size of iridium species revealed by HRTEM and TEM images in Fig. 2 based on our previous discussion [18,35,40].

It is also interesting to note that the magnesia modification on Ta_3N_5 can effectively suppress the oxidation of I^- ions (Fig. 1b). To get insight into the inhibition of I^- ions oxidation, we compare the adsorption ability of I^- ions on the pristine Ta_3N_5 and MgO/Ta_3N_5 by UV–vis absorption spectra. Based on the measurement of absorption and calibration curves of NaI by UV spectrophotometry (Fig. S10), the adsorbed amount of I^- ions on both samples are then calculated and figured in Fig. 3a, from which the MgO/Ta_3N_5 sample shows obviously decreased adsorption ability of I^- ions compared to the pristine Ta_3N_5. Furthermore, the amount of I^- ions adsorbed is decreased with increasing the mass ratio of MgO:Ta_3N_5 (Fig. 3b). The suppression of I^- ions on the magnesia-modified sample compared to the pristine Ta_3N_5 one is very similar to that of previous publications [13,18], where the adsorption of I^- ions on the surface of rutile TiO_2 and WO_3 were found to be suppressed. Since the adsorption is one of the most crucial steps towards the catalysis, the inefficient adsorption of I^- ions on the MgO/Ta_3N_5 sample is expected to be responsible for the suppressed oxidation of I^- ions and the enhanced O_2 evolution activity. All the above results prove that the magnesia modification promotes the dispersion of deposited iridium and suppresses the adsorption and oxidation of I^- ions (a competing reaction of water oxidation), leading to the enhanced performance of water oxidation.

3.2. H_2-evolving reaction and inhibition of IO_3^- ions reduction

The ZrO_2/TaON sample was employed as a HEP, together with platinum as the reduction cocatalyst. If needed, Cr_2O_3 was photodeposited on the surface of platinum for discussion. The basic processes for H_2 evolution can be described by following equations of 3 and 4 in Scheme 1.

$$\text{Photocatalyst} + h\nu\ (> \text{band gap energy}) \rightarrow e^- + h^+$$

$$2H^+ + 2e^- \rightarrow H_2 \quad (3)$$

$$I^- + 6\,h^+ + 3H_2O \rightarrow IO_3^- + 6H^+ \quad (4)$$

Firstly, the H_2 evolution on the ZrO_2/TaON-based photocatalysts were evaluated under various concentrations of I^- ions added. As shown in Fig. 4a, a pseudo-linear increase of H_2 evolution rate can be similarly observed for the samples with and without surface modification of Cr_2O_3 in the concentration range of 0–1 mM. Furthermore, after the surface Cr_2O_3 modification, the H_2 evolution rate is significantly improved in all the investigated concentration range of I^- ions. Since the deposited Cr_2O_3 has no ability to catalyze the I^- ions oxidation or proton reduction, it is deduced that the promoted H_2 evolution rate may result from prevention of the reduction of IO_3^- ions. To test our speculation, we thus examined the H_2 evolution rate in the presence of 4 mM NaI together with different concentrations of $NaIO_3$. Fig. 4b gives its representative results on the ZrO_2/TaON-based samples, from which the H_2 evolution rate is decreased with increasing the concentration of $NaIO_3$, indicating that the reduction of IO_3^- ions (the reaction 6 in Scheme 1) does really compete with the proton reduction (the reaction 3 in Scheme 1) to consume photogenerated electrons. Comparatively, the presence of Cr_2O_3 can dull the influence from IO_3^- ions and make the photocatalyst exhibit a better tolerance to IO_3^- ions. Compared with the sharp decrease of H_2 evolution rate (below 0.5 μmol/h after the addition of 0.1 mM IO_3^- ions) on the single platinum-deposited sample, the sample with further surface modification of Cr_2O_3 (Pt/Cr_2O_3) can obviously inhibit the decreasing extent, demonstrating the feasibility of Cr_2O_3 deposition in suppressing the competing reaction. The inhibition of IO_3^- ions reduction can be further confirmed by the electrochemical results (Fig. 4c), where the onset potential on the Pt-ZrO_2/TaON is remarkably negatively shifted after the deposition of Cr_2O_3. It should be pointed out that the Cr_2O_3 itself is not active for reduction of proton or IO_3^- ions based on their similar electrochemical current of ZrO_2/TaON and Cr_2O_3-ZrO_2/TaON electrodes (not given). And the much better electrochemical current on the Pt-ZrO_2/TaON electrode mainly originates from the IO_3^- ions reduction that is much easier than proton reduction.

Subsequently, a series of characterizations were conducted for the HEP. The basic diffraction structure of ZrO_2/TaON was characterized and confirmed by XRD (Fig. S11a). According to the UV–vis DRS (Fig. S11b), the absorption edge of *ca.* 520 nm is observed for the ZrO_2/TaON sample. The existed state of photodeposited chromium can be deduced to be chromium (III) oxide according to the binding energy

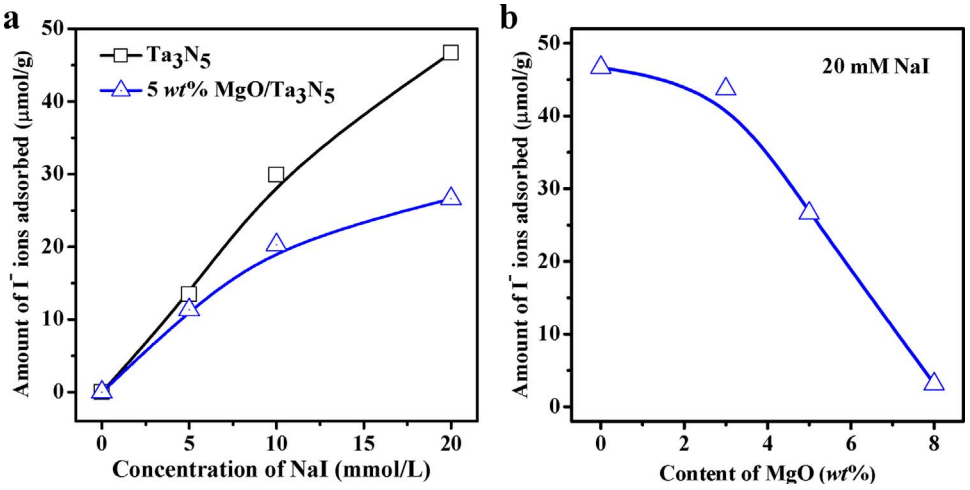

Fig. 3. (a) Adsorption properties of iodide (I^-) ions on Ta_3N_5-based photocatalysts; (b) Adsorption properties of iodide (I^-) ions on different amount of MgO modified Ta_3N_5 photocatalysts.

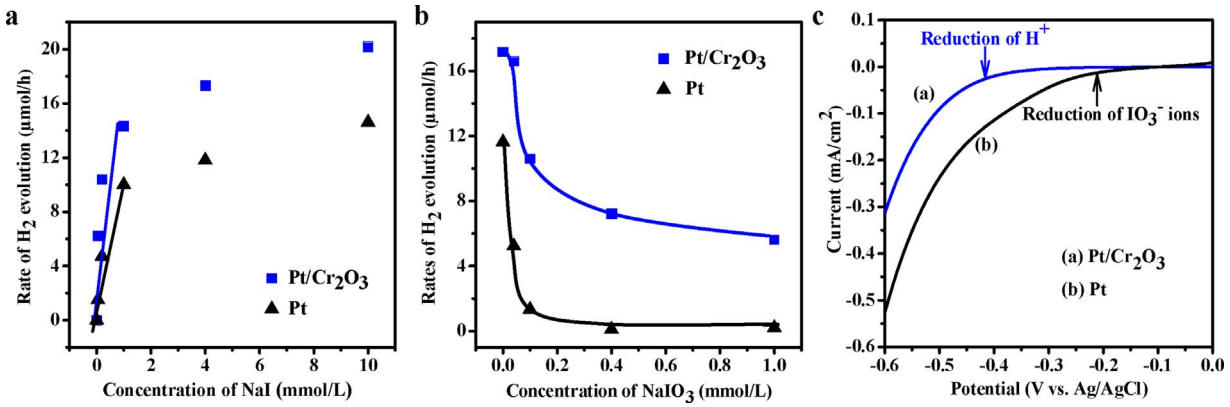

Fig. 4. (a) H_2-evolving reaction kinetics as a function of the concentration of I^- ions added on the Pt-ZrO_2/TaON and Pt/Cr_2O_3-ZrO_2/TaON photocatalysts[a]. (b) Influence of the concentration of IO_3^- ions on the initial rate of H_2 evolution for ZrO_2/TaON[b]. (c) *I–V* characteristics of Pt-ZrO_2/TaON electrodes with and without Cr_2O_3 coating in the aqueous solution containing 5 mM $NaIO_3$.

[a] Reaction conditions: 0.06 g catalyst; 0.7 *wt*% Pt or 0.7 *wt*% Pt/Cr_2O_3 (Cr/Pt mass ratio = 1.5); aqueous NaI solution (100 mL); 300 W xenon lamp (λ ≥ 420 nm), Pyrex top-irradiation type, 1 h reaction time.

[b] Reaction conditions: 0.06 g catalyst; 0.7 *wt*% Pt or 0.7 *wt*% Pt/Cr_2O_3 (Cr/Pt mass ratio = 1.5); aqueous NaI solution (100 mL, 4 mM); 300 W xenon lamp (λ ≥ 420 nm), Pyrex top-irradiation type, 1 h reaction time.

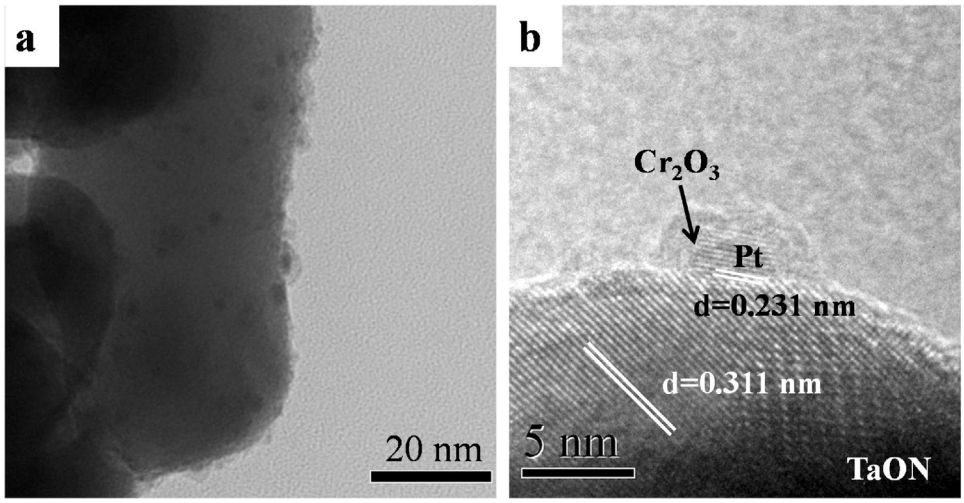

Fig. 5. TEM (a) and HRTEM (b) images of Pt/Cr_2O_3-ZrO_2/TaON.

(576.7 eV) of Cr 2*p* XPS spectrum in Fig. S12 [41]. As seen in the TEM image of Fig. 5a, the particle size of deposited platinum on the ZrO_2/TaON sample is mainly located in the range of 2–5 nm. And the HRTEM image (Fig. 5b) reveals that the photodeposited chromium is mainly on the surface of deposited Pt to form core/shell structure [36]. To date, the exact reason of the inhibition effect is still under investigation, but it is reasonably proposed that the Cr_2O_3 shell may suppress the undesirable reduction of IO_3^- ions via preventing the IO_3^- ions from diffusing onto the surface of the deposited Pt cocatalyst, as similar to preventing reduction of the O_2 molecule during the water splitting process [36,42]. It should be pointed out that the Cr_2O_3 shell does not make an obvious influence on the transportation of electron according to the TRIR results (Fig. S13), in which the lifetime of carriers on the Pt/Cr_2O_3-ZrO_2/TaON is similar to that of Pt-ZrO_2/TaON.

3.3. Construction of photocatalytic Z-Scheme OWS system

Encouraged by inhibiting competing reactions of both H_2- and O_2-evolving parts, we attempt to fabricate Z-scheme OWS system by employing pristine and surface modified HEPs and OEPs using the mixture of IO_3^- and I^- ions as redox shuttle mediator. Table 1 summarizes the series of experimental results. If we employ the Ir-Ta_3N_5 as an OEP, Z-scheme OWS is infeasible regardless of the HEPs with or without Cr_2O_3 modification (entry 1 and 2). In these cases, no obvious O_2 evolution can be detected except for the formation of H_2. This is mainly ascribed to the strong competing reaction of I^- ions oxidation (the reaction 5 in Scheme 1) on the Ir-Ta_3N_5 sample (Fig. 1b). When we employ the Ir-MgO/Ta_3N_5 samples as an OEP, the formation of O_2 can be obviously detected (entries 3–11). Meanwhile, no H_2 is evolved when the HEPs are free of surface modification of Cr_2O_3 nanolayer (entry 1 and 3), as mainly originates from the competing reaction of IO_3^- ions reduction (the reaction 6 in Scheme 1), which is much easier than the proton reduction. Interestingly, when the HEP and OEP are simultaneously modified by Cr_2O_3 and magnesia, respectively (it means simultaneously suppressing the competing reactions of both H_2-evolving and O_2-evolving sides), both H_2 and O_2 evolutions can be detected (entries 4–11) in the coexistence of IO_3^- and I^- ions. However, the molar ratio of H_2:O_2 is strongly dependent on the concentration ratio of NaI and $NaIO_3$ added. For example, if the concentration of NaI is fixed (entries 4–7), the molar ratio of H_2:O_2 formed will be decreased with increasing amount of $NaIO_3$ added, and the stoichiometric ratio of 2:1 is observed in the case of entry 6. Oppositely, if the concentration of $NaIO_3$ is fixed (entries 8–11), the molar ratio of H_2:O_2 formed will be gradually enhanced with increasing amount of NaI added, and the stoichiometric ratio of 2:1 can be detected in the case of entry 10. Based on the above activity results, it is reasonable to conclude that the Z-scheme OWS systems can be fabricated by suppressing both competing reactions originating from IO_3^- ions reduction and I^- ions oxidation on the H_2-

Table 1
Comparison of Z-scheme water splitting performances using different photocatalysts and redox compositions under visible light irradiation [a].

Entries	H_2-evolving photocatalyst	O_2-evolving photocatalyst	Addition of redox		Rate/μmol/h	
			NaI	$NaIO_3$	H_2	O_2
1	Pt-ZrO_2/TaON	Ir-Ta_3N_5	4.0	1.0	n.d.	n.d.
2	Pt/Cr_2O_3-ZrO_2/TaON	Ir-Ta_3N_5	4.0	1.0	15.5	n.d.
3	Pt-ZrO_2/TaON	Ir- MgO/Ta_3N_5	4.0	1.0	n.d.	2.5
4	Pt/Cr_2O_3-ZrO_2/TaON	Ir- MgO/Ta_3N_5	4.0	0.0	11.3	0.2
5	Pt/Cr_2O_3-ZrO_2/TaON	Ir- MgO/Ta_3N_5	4.0	0.25	9.5	1.0
6	Pt/Cr_2O_3-ZrO_2/TaON	Ir- MgO/Ta_3N_5	4.0	1.0	5.0	2.5
7	Pt/Cr_2O_3-ZrO_2/TaON	Ir- MgO/Ta_3N_5	4.0	2.0	2.0	4.4
8	Pt/Cr_2O_3-ZrO_2/TaON	Ir- MgO/Ta_3N_5	0.0	0.25	0.1	8.0
9	Pt/Cr_2O_3-ZrO_2/TaON	Ir- MgO/Ta_3N_5	1.0	0.25	2.0	3.0
10	Pt/Cr_2O_3-ZrO_2/TaON	Ir- MgO/Ta_3N_5	2.0	0.25	4.5	2.2
11	Pt/Cr_2O_3-ZrO_2/TaON	Ir- MgO/Ta_3N_5	3.0	0.25	6.8	1.5

[a] Reaction conditions: 120 mg HEP; 0.7 *wt*% Pt or 0.7 *wt*% Pt/Cr_2O_3 (Cr/Pt mass ratio = 1.5); 40 mg OEP; 1.0 *wt*% Ir; 100 mL aqueous solution; 300 W xenon lamp (λ ≥ 420 nm), Pyrex top-irradiation type.

evolving and O_2-evolving sides, respectively. Moreover, the Z-scheme OWS with stoichiometric H_2 and O_2 can be reached in some specific conditions (entry 6 and 10), where both HEP and OEP are simultaneously surface modified, and mixture of NaI and $NaIO_3$ with suitable ratio should be used as a redox mediator. This indicates that the effective inhibition of competing reactions and the balance between H_2- and O_2-evolving reaction kinetics are crucial for the fabrication of Z-scheme OWS system when we employ the mixture of IO_3^- and I^- ions as the redox mediator. Time course result of the typical sample demonstrates that the system is stable in the tested period (Fig. S14). The no obvious changes of XRD patterns for the HEP and OEP before and after the photocatalytic reaction (Fig. S15) demonstrates their structural stability during the experimental region.

Above all, the construction of IO_3^-/I^- mediator-based Z-scheme OWS systems not only depends on the structure control of photocatalyst itself for promotion of charge separation as well as reaction kinetics, but also needs to overcome the corresponding undesirable competing reactions caused by the shuttle ions. Here the magnesia surface modification is found to favor both of them, and the deposition of Cr_2O_3 shell is demonstrated to be effectively prevent the reduction of IO_3^- ions. As an integral contribution, we can finally fabricate effective Z-scheme OWS systems using mixture of IO_3^- and I^- ions as the redox mediator.

4. Conclusion

Here we give a detailed discussion on how to construct an effective Z-scheme OWS system using mixture of IO_3^- and I^- ions as the redox mediator with an emphasis on surface modification. Inhibition of competing reactions caused by the redox mediator ions and promotion of reaction kinetics on both OEP and HEP are found to be the key issues. Suitable surface modification on the OEP and HEP is demonstrated to be the feasible strategy towards the final goal. Meanwhile, the magnesia modification on the Ta_3N_5 is found to promote the dispersion of deposited iridium cocatalyst and inhibit the oxidation of I^- ions (the competing reaction of water oxidation), resulting in improving the reaction kinetics of water oxidation. The surface modification of Cr_2O_3 on the deposited metallic Pt can prevent the reduction of IO_3^- ions (the competing reaction of proton reduction). Based on the inhibition of competing reactions and improvement of the reaction kinetics, we finally fabricate a Z-scheme OWS system using mixture of IO_3^- and I^- ions as the redox mediator. Inhibiting competing reactions of redox mediators by surface modification is expected to be a blueprint of fabricating Z-scheme OWS systems for solar energy conversion, and more effective ways of surface modification are needed to be developed for enhanced Z-scheme OWS performance.

Acknowledgements

This work was financially supported by National Natural Science Foundation of China (21633009, 21373210, 21522306), the Basic Research Program of China (973 Program: 2014CB239403). F. Zhang thanks the priority support from the “Hundred Talents Program” of Chinese Academy of Sciences.

Appendix A. Supplementary data

Supplementary data associated with this article can be found, in the online version, at http://dx.doi.org/10.1016/j.apcatb.2017.10.041.

References

[1] A. Kudo, Y. Miseki, Soc. Rev. 38 (2009) 253–278.
[2] X. Chen, S. Shen, L. Guo, S. Mao, Chem. Rev 110 (2010) 6503–6570.
[3] F. Osterloh, Chem. Soc. Rev. 42 (2013) 2294–2320.
[4] S. Chen, T. Takata, K. Domen, Nat. Rev. Mater. 2 (2017) 1–17.
[5] Y. Ma, X. Wang, Y. Jia, X. Chen, H. Han, C. Li, Chem. Rev. 114 (2014) 9987–10043.
[6] R. Marschall, L. Wang, Catal. Today 225 (2014) 111–135.
[7] Y. Wang, X. Wang, M. Antonietti, Angew. Chem. Int. Ed. 51 (2012) 68–89.
[8] D. Fabian, S. Hu, N. Singh, F. Houle, T. Hisatomi, K. Domen, F. Osterloh, S. Ardo, Energy Environ. Sci. 8 (2015) 2799–3050.
[9] G. Zhang, Z. Lan, L. Lin, S. Lin, X. Wang, Chem. Sci. 7 (2016) 3062–3066.
[10] C. Pan, T. Takata, M. Nakabayashi, T. Matsumoto, N. Shibata, Y. Ikuhara, K. Domen, Angew. Chem. Int. Ed. 54 (2015) 1–6.
[11] K. Maeda, ACS Catal. 3 (2013) 1486–1503.
[12] A. Kudo, MRS Bull. 36 (2011) 32–38.
[13] R. Abe, Bull Chem, Soc. Jpn. 84 (2011) 1000–1030.
[14] R. Abe, K. Sayama, K. Domen, H. Arakawa, Chem. Phys. Lett. 344 (2001) 339–344.
[15] S. Chen, Y. Qi, T. Hisatomi, Q. Ding, T. Asai, Z. Li, S. Ma, F. Zhang, K. Domen, C. Li, Angew. Chem. Int. Ed. 54 (2015) 498–8501.
[16] K. Maeda, M. Higashi, D. Lu, R. Abe, K. Domen, J. Am. Chem. Soc. 132 (2010) 5858–5868.
[17] K. Maeda, R. Abe, K. Domen, J. Phys. Chem. C 115 (2011) 3057–3064.
[18] M. Tabata, K. Maeda, M. Higashi, D. Lu, T. Takata, R. Abe, K. Domen, Langmuir 26 (2010) 9161–9165.
[19] K. Maeda, D. Lu, K. Domen, ACS Catal. 3 (2013) 1026–1033.
[20] W. Zhao, K. Maeda, F. Zhang, T. Hisatomi, K. Domen, Phys. Chem. Chem. Phys. 16 (2014) 12051–12056.
[21] T. Kato, Y. Hakari, S. Ikeda, Q. Jia, A. Iwase, A. Kudo, J. Phys, Chem. Lett. 6 (2015) 1042–1047.
[22] H. Fujito, H. Kunioku, D. Kato, H. Suzuki, M. Higashi, H. Kageyama, R. Abe, J. Am. Chem. Soc. 138 (2016) 2082–2085.
[23] K. Sayama, K. Mukasa, R. Abe, Y. Abe, H. Arakawa, Chem. Commun (2001) 2416–2417.
[24] S. Tanigawa, H. Irie, Appl. Catal. B 108 (2016) 1–5.
[25] R. Abe, K. Shinmei, N. Koumura, K. Hara, B. Ohtani, J. Am. Chem. Soc. 135 (2013) 16872–16884.
[26] D. Martin, P. Reardon, S. Moniz, J. Tang, J. Am. Chem. Soc. 136 (2014) 12568–12571.
[27] W. Wang, J. Chen, C. Li, W. Tian, Nat. Commun. 5 (2014) 4647.
[28] Y. Sasaki, H. Kato, A. Kudo, J. Am. Chem. Soc. 135 (2013) 5441–5449.
[29] J. Yan, H. Wu, H. Chen, Y. Zhang, F. Zhang, S. Liu, Appl. Catal. B 191 (2016) 103–137.
[30] M. Higashi, R. Abe, T. Takata, K. Domen, Chem. Mater 21 (2009) 1543–1549.
[31] R. Abe, T. Takata, H. Sugihara, K. Domen, Chem. Commun. (2005) 3829–3831.
[32] R. Abe, M. Higashi, K. Domen, ChemSusChem 4 (2011) 228–237.
[33] K. Maeda, K. Domen, J. Phys, Chem. Lett. 1 (2010) 2655–2661.
[34] S. Chen, S. Shen, G. Liu, Y. Qi, F. Zhang, C. Li, Angew. Chem. Int. Ed. 54 (2015) 3047–3051.
[35] S. Chen, Y. Qi, Q. Ding, Z. Li, J. Cui, F. Zhang, C. Li, J. Catal 339 (2016) 77–83.
[36] K. Maeda, N. Sakamoto, T. Ikeda, H. Ohtsuka, A. Xiong, D. Lu, M. Kanehara, T. Teranishi, K. Domen, Chem. Eur. J. 16 (2010) 7750–7759.
[37] Z. Wang, Y. Qi, C. Ding, D. Fan, G. Liu, Y. Zhao, C. Li, Chem. Sci. 7 (2016) 4391–4399.
[38] S. Ma, K. Maeda, R. Abe, K. Domen, Energy Environ. Sci. 5 (2012) 8390–8397.
[39] F. Bernardi, J. Scholten, G. Fecher, J. Dupont, J. Morais, Chem. Phys. Lett. 479 (2009) 113–116.
[40] R. Isaifan, S. Ntais, E. Baranova, Appl. Catal. A 464 (2013) 87–94.
[41] E. Desimoni, C. Malitesta, P. Zambonim, J. Rivière, Surf. Interface Anal. 13 (1988) 173–179.
[42] F. Dionigi, P. Vesborg, T. Pedersen, O. Hansen, S. Dahl, A. Xiong, K. Maeda, K. Domen, I. Chorkendorff, J. Catal. 292 (2012) 26–31.